Hollow Nanostructures

DOI: 10.1002/ange.201308589

Well-Defined Metal–Organic Framework Hollow Nanocages**

*Zhicheng Zhang, Yifeng Chen, Xiaobin Xu, Jingchao Zhang, Guolei Xiang, Wei He, and Xun Wang**

Abstract: *Metal–organic frameworks (MOFs) have demonstrated great potentials in a variety of important applications. To enhance the inherent properties and endow materials with multifunctionality, the rational design and synthesis of MOFs with nanoscale porosity and hollow feature is highly desired and remains a great challenge. In this work, the formation of a series of well-defined MOF (MOF-5, Fe^{II}-MOF-5, Fe^{III}-MOF-5) hollow nanocages by a facile solvothermal method, without any additional supporting template is reported. A surface-energy-driven mechanism may be responsible for the formation of hollow nanocages. The addition of pre-synthesized poly(vinylpyrrolidone)- (PVP) capped noble-metal nanoparticles into the synthetic system of MOF hollow nanocages yields the yolk–shell noble metal@MOF nanostructures. The present strategy to fabricate hollow and yolk–shell nanostructures is expected to open up exciting opportunities for developing a novel class of inorganic–organic hybrid functional nanomaterials.*

Metal–organic frameworks (MOFs) are definitely one of the most fascinating research fields emerging in most recent decades.[1–5] MOFs assembled by the principle of coordination chemistry, where metal centers/clusters are bridged by functional organic ligands, with tunable porous structures have been attracting considerable interests because of their intrinsic properties and potential applications in gas sorption,[6,7] separations,[5,8] catalysis,[9–11] drug delivery,[12,13] optics,[14,15] and sensing.[16,17] Since they are usually crystalline materials with irregular shapes which may limit their further applications, recent efforts have been made to tailor their shapes and sizes, referring to the concept of nanosynthesis. For example, Mirkin and Oh[18] developed the strategy of infinite coordination polymer (ICP), the structure of which is amorphous and has the advantages in achieving shape and size control while keeping the inorganic–organic backbone. Huo and co-workers[19] endowed MOFs with different functions by incorporating noble-metal nanocrystals inside micro-sized MOFs. Tang and co-workers[20] capped Au nanocrystals with MOF layers to enhance their sensing properties. However, as compared with the rich synthetic chemistry of nanocrystals, much more efforts in synthetic strategy are apparently still needed to push forward the development of nano-MOFs.

So far, hollow structured inorganic nanomaterials (such as metals[21] and metal oxides[22]) have received much attention because of their intriguing properties such as low density, high surface area, material economy, and cost reduction compared with their solid counterparts, and thus find wide use in many important fields. Various fabrication procedures for hollow structures have been developed involving templates,[21a,22a,f] Kirkendall effect,[22b,c] galvanic replacement,[21b,22d] Ostwald ripening,[21c] reduction of metal oxides,[21d] and so on. On the contrary, very scarce reports concern about the construction of MOF hollow structures. The current synthetic progresses are mainly confined to hollow spheres with micrometer-range sizes,[23] relatively wide size distribution and not well-defined shapes,[24] as compared with the finely tunable structures of their inorganic hollow nanocage counterparts. Herein, we demonstrate that a series of well-defined MOF hollow nanocages including MOF-5, Fe^{II}-MOF-5, Fe^{III}-MOF-5, and Fe^{III}-ICP (Scheme 1) can be solvothermally prepared in high yields using 1,4-benzenedicarboxylic acid (H_2BDC) as organic linkers, zinc and ferric ions as metallic nodes, poly(vinylpyrrolidone) (PVP) as stabilizing reagent, and *N*,*N*-dimethylformamide (DMF) or *N*,*N*-dimethylacetamide (DMAC)–ethanol as mixed solvent. An interesting shape evolution process from uniform MOF nanocrystals with concave and high-energy facets into hollow nanocages was observed along with prolonging of reaction time, based on which we suggest that a surface-energy-driven mechanism may be responsible for the formation of these hollow

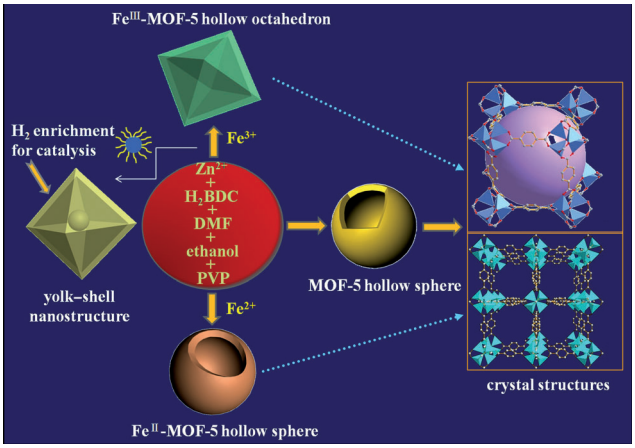

Scheme 1. A series of well-defined MOF hollow nanocages.

[*] Z. C. Zhang, Y. F. Chen, X. B. Xu, J. C. Zhang, G. L. Xiang, W. He, Prof. X. Wang
Department of Chemistry, Tsinghua University
Beijing, 100084 (P. R. China)
E-mail: wangxun@mail.tsinghua.edu.cn

[**] This work was supported by the NSFC (grant numbers 91127040 and 21221062), the CPSF (grant number 2013M540085), and the State Key Project of Fundamental Research for Nanoscience and Nanotechnology (grant number 2011CB932402).

Supporting information for this article is available on the WWW under http://dx.doi.org/10.1002/anie.201308589.

nanocages. Impressively, by adding the pre-synthesized PVP-capped noble-metal nanoparticles into the synthetic solution of MOF (ICP) hollow nanocages, we successfully prepared the yolk–shell noble-metal@MOF (ICP) nanostructures. These yolk–shell structures were found to show highly enhanced catalytic performance in the liquid-phase selective hydrogenation of 1-chloro-2-nitrobenzene relative to the pure yolk.

The morphology and structural features of as-prepared MOF-5 hollow nanospheres were characterized by transmission electron microscopy (TEM). The product assumes a roughly spherical and hollow shape with an average diameter of 135 nm (Figure 1 a). By close observation, each hollow nanosphere is composed of numerous small nanoparticles (NPs) with sub-10 nm sizes (Figure 1 a, inset). The powder X-ray diffraction (PXRD) pattern of the hollow nanospheres matches well with that of cubic crystalline MOF-5 (Figure 1 c), indicating the successful synthesis of nanosized MOF-5 relative to its traditional micrometer-scale structure. Impressively, the addition of $(NH_4)_2SO_4{\cdot}FeSO_4{\cdot}6H_2O$ into the reaction solution of MOF-5 hollow nanospheres yielded Fe^{II}-MOF-5 hollow nanospheres (Figure 1 b), suggesting the coordination flexibility of the polymeric architectures. PXRD results show that these hollow nanospheres retained the MOF-5 crystalline lattice (Figure 1 c). Discrepancies in peak intensities arise from preferential orientation because we avoided grinding the samples so as to preserve their structural integrity. The high-angle annular dark-field scanning TEM (HAADF-STEM) image (Figure 1 d) further confirms the hollow nature of Fe^{II}-MOF-5. Elemental mapping by energy-dispersive X-ray spectroscopy (EDS) shows that the elements C, O, Fe, and Zn are homogeneously distributed throughout the whole nanoparticle (Figure 1 d, inset). Nevertheless, the survey XPS spectrum verify the formation of Fe^{3+}-substituted MOF-5 (see Figure S1 in the Supporting Information), suggesting that Fe^{2+} may be oxidized to Fe^{3+} before coordination reaction in our synthetic system. In this study, in contrast to the homometallic MOFs, the heterometallic MOFs that bear two different metals will attract special attention because of potential synergic effects of different metals within one assembly and a variety of advanced applications.[25]

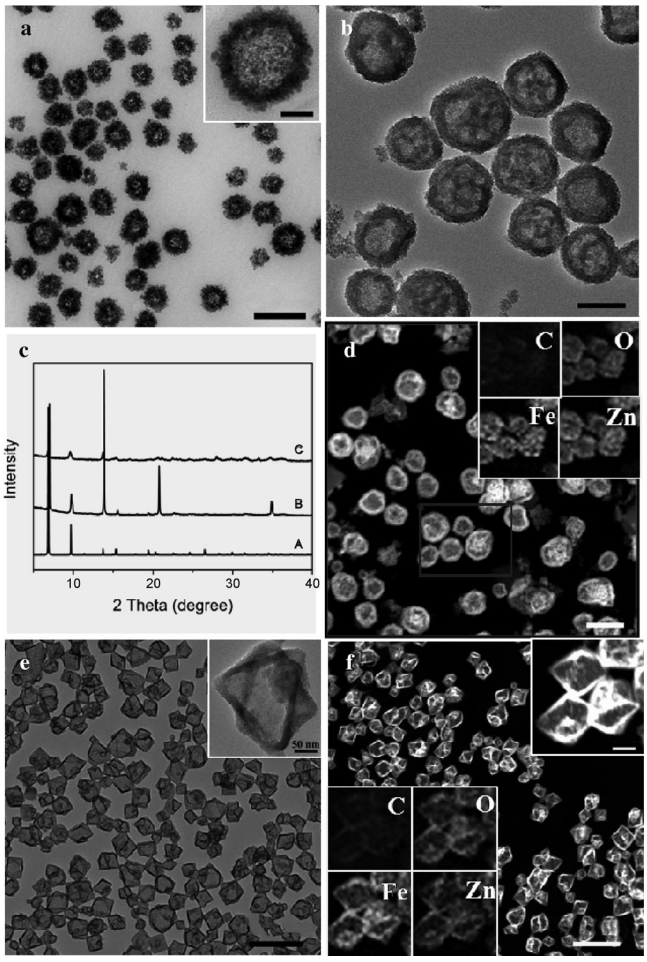

Figure 1. a) TEM image of MOF-5 hollow nanospheres (scale bar 200 nm; scale bar in the inset 50 nm). b) TEM image of Fe^{II}-MOF-5 hollow nanospheres (scale bar 100 nm). c) XRD patterns of cubic crystalline MOF-5 (A), MOF-5 hollow nanospheres (B), and Fe^{II}-MOF-5 hollow nanospheres (C). d) HAADF-STEM image of Fe^{II}-MOF-5 hollow nanospheres (scale bar 200 nm). The inset in (d) shows corresponding EDS mapping images of Fe^{II}-MOF-5. e) TEM (scale bar 500 nm) and f) HAADF-STEM images (scale bar 500 nm) of Fe^{III}-MOF-5 hollow octahedral nanostructures. The insets in (e; scale bar 50 nm) and (f; scale bar 100 nm) are high-magnification TEM and EDS mapping images of Fe^{III}-MOF-5, respectively.

Interestingly, when we used Fe^{III} instead of Fe^{II}, Fe^{III}-MOF-5 could also be obtained, the PXRD pattern of which matches well with that of cubic crystalline MOF-5 (Figure S2). However, the products were heavily aggregated mainly in the shape of hollow octahedral nanostructures (Figure S3). Fortunately, it was found that the addition of PVP would lead to the formation of uniform Fe^{III}-MOF-5 hollow octahedral nanostructures (Figure 1 e,f). This indicates that PVP functions as stabilizing reagent to protect and disperse the NPs. EDS mapping images (Figure 1 f, inset) reveal the homogeneous distribution of elements C, O, Fe, and Zn in the nanoparticle. The survey XPS spectrum shows that the samples are also made of Fe, Zn, C, N, and O (Figure S4). Furthermore, it was found that solvents played an important role in determining the final structure of the Fe^{III}-MOF-5. Compared with the synthetic process of Fe^{III}-MOF-5, when DMF was substituted with DMAC, well-defined hollow octahedral nanostructures could be produced. The PXRD result reveals that the sample is typical amorphous and not crystalline (Figure S5), which may refer to an infinite coordination polymer (marked as Fe^{III}-ICP).[18] The representative electron microscopic images of the product are illustrated in Figure 2. As shown in the scanning electron microscopy (SEM) image (Figure 2 a), the product consists of uniform octahedral nanostructures with an average edge length of 240 nm and the selectivity to octahedra is higher than 80 %. Careful observation by high-magnification SEM shows that the surface of these octahedral nanostructures is very rough (Figure 2 a, inset), indicating that these octahedral nanostructures are constructed by many small NPs with diameters below 10 nm. Furthermore, some broken octahedral particles appear in the sample (Figure 2 a, bottom-left inset), disclosing their hollow structure. The TEM image

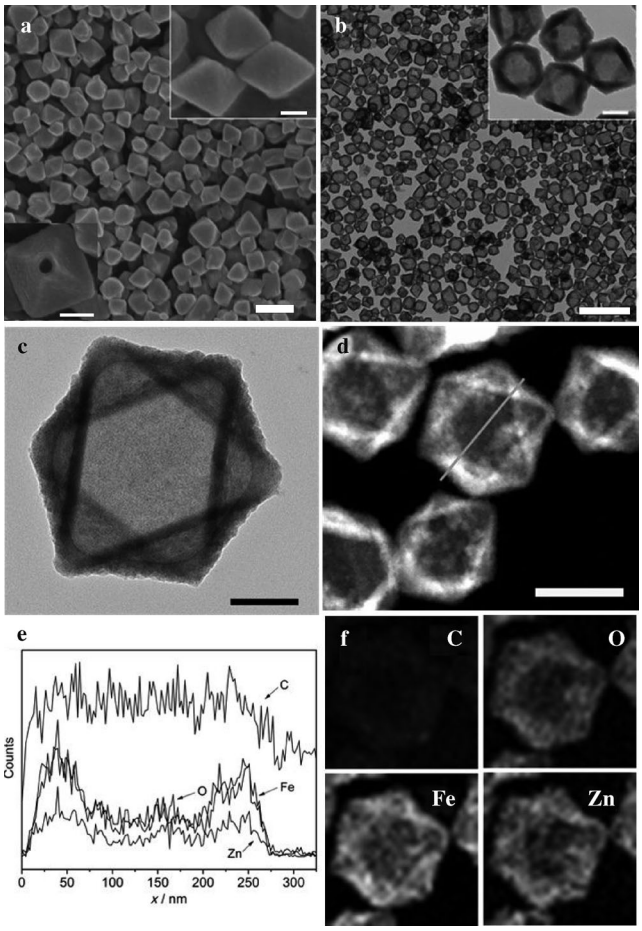

Figure 2. a) SEM (scale bar 500 nm), b,c) TEM (scale bars 1 μm and 100 nm, respectively), and d) HAADF-STEM images (scale bar 200 nm) of as-obtained Fe^{III}-ICP hollow octahedral nanostructures. The insets in (a; scale bars in both insets 100 nm) and (b; scale bar 100 nm) show corresponding high-magnification SEM and TEM images, respectively. e) EDS line scanning profiles, and f) EDS mapping images of a single nanoparticle as labeled in (d).

further confirms the hollow feature of these octahedral nanostructures (Figure 2b,c), which can also be observed from the HAADF-STEM image (Figure 2d) and EDS line scanning profiles across an individual particle (Figure 2e). The EDS mapping images show that the elements C, O, Fe, and Zn are uniformly dispersed in the nanoparticle (Figure 2f).

The chemical composition of Fe^{II}-MOF-5, Fe^{III}-MOF-5, and Fe^{III}-ICP hollow nanostructures was determined by elemental analysis (see the Experimental Section for details). FT-IR spectra (Figure S6) of Fe^{III}-ICP hollow octahedral nanostructures verify the coordination of the carboxylate groups to metal ions, as evidenced by a red shift in the carboxylate stretching frequency to 1563 cm^{-1} from 1680 cm^{-1} for uncoordinated H_2BDC, which is consistent with the previous report.[26] On the basis of both FT-IR and XPS (Figure S7) analyses, the possible coordination environment of Fe^{III} and Zn^{II} ions with BDC in heterometallic Fe^{III}-ICP hollow octahedral nanostructures was depicted in Figure S8. Thermogravimetric (TG) analysis of Fe^{III}-ICP hollow octahedral nanostructures in nitrogen shows that the hollow octahedral nanostructures do not exhibit significant weight loss up to at least 350 °C (Figure S9), which can be attributed to the solvent liberation.[27] Additionally, it was found that the hollow octahedral nature of Fe^{III}-ICP does not change in most organic solvents (DMF, DMAC, acetone, methanol, alcohol, and nonpolar hydrocarbons), water, and the dried state.

To further gain an insight into the evolution process of Fe^{III}-ICP hollow octahedral nanostructures, we carried out the time-dependent experiments and monitored the solvothermal process by SEM and TEM as shown in Figure 3, when

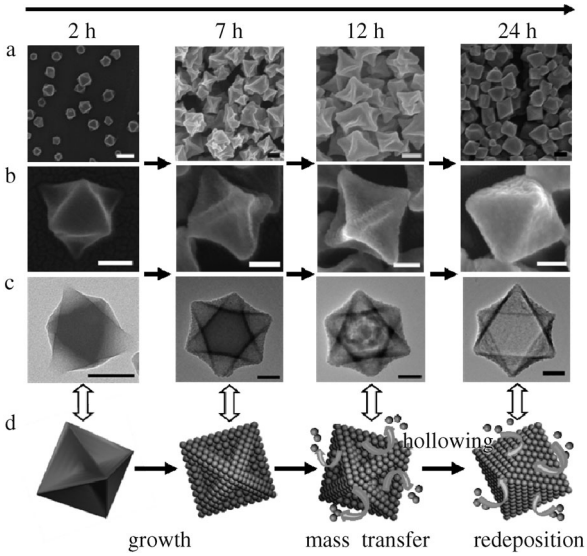

Figure 3. a,b) SEM and c) TEM images of Fe^{III}-ICP collected at different reaction times. Scale bar: a) 200 nm; b,c) 100 nm. d) Proposed formation process of Fe^{III}-ICP hollow octahedral nanostructures.

the reaction time was shortened to 2 h. In the TEM image, it is seen that the reaction product consists of uniform octahedral nanostructures with an average side length of 150 nm. The TEM image shows that the octahedral NPs show darker contrast in the middle region as compared with the edges, indicating the possible presence of concave features in the NPs. SEM images further confirm that each face of the NPs is concave and smooth, which can be clearly observed from the corresponding model. Then, these NPs were found to grow continuously within 5 h. At 7 h, the side length of the concave octahedral NPs reaches approximately 240 nm. Meanwhile, the surface of the NPs becomes relatively rough. To further clearly characterize the surface structure and elemental distribution of this intermediate product, the typical electron microscopic images of the sample are shown in Figure S10. By close observation, the surface of the sample can be visualized as an excavated octahedron with a trigonal pyramid excavated at the center of each face of the octahedron (Figure S10a–c). Both EDS line scanning profiles (Figure S10c, inset) and mapping images (Figure S10d) demonstrate the homogeneous distribution of C, O, Fe, and Zn elements. As the reaction time was extended to 12 h, it was found that small cavities begin to form inside the solid concave octahedral NPs,

as confirmed by TEM. As the reaction proceeded, the solid evacuation became much more obvious. For the sample at 24 h, perfect hollow octahedral NPs with a size of 240 nm were ultimately produced. Note that the surface of the NPs was not concave but relatively flat. We deduce that the deposition of small NPs from inside finally leads to the formation of hollow octahedral nanostructures with a flat surface. Further prolonging the reaction time to 36 h, no significant change in the size and surface structure was observed, implying that the reaction was complete. During the solvothermal process, we used EDS to determine the molar ratio of Fe to Zn elements. The results showed that the molar ratio of Fe to Zn was almost unchanged. This indicates that the Kirkendall effect could be excluded in the formation process of hollow octahedral NPs, which has usually been used to explain the formation mechanism of hollow structures.[22b,c] Based on the above experimental facts, we propose that the surface-energy-driven mechanism may be responsible for the formation of these hollow nanostructures. First, because of the coordination reaction between metal ions and organic ligands, a large number of small coordination polymer units nucleate from solution and aggregate quickly to minimize the surface energy.[24] Meanwhile, in the initial stage of particle formation, owing to the high concentration of metal ions and organic ligands, the growth units are rapidly formed, allowing rapid fusion and growth using coordination chemistry.[28] At this time, the chemical potential of growth units in solution is quite high, thus yielding a high supersaturation. It has been proposed that high supersaturation will result in the formation of NPs with high surface-energy faces.[29] In this work we have observed the formation of concave octahedra with high surface energies, which is a direct result of high supersaturation or high chemical potential energy of the initial reaction system. After then, as the concentration of metal ions and organic ligands decreases, the supersaturation of growth units will also decrease, which finally leads to the formation of hollow octahedra with low surface energy. Over time, an inside–out formation process takes place to reduce their high surface energy.[24,27] To further validate the proposed formation mechanism above, time sequential evolution experiments were performed during the solvothermal process for MOF-5 hollow nanospheres, Fe^{II}-MOF-5 hollow nanospheres, and Fe^{III}-MOF-5 hollow octahedral nanostructures. The results show that similar shape evolution process from solid to hollow structures could be observed (Figure S11). Based on the previous work,[24,27] we suggest that inner crystallites dissolve and migrate out to reduce their higher surface energies, thus the hollow cavities inside the spheres or octahedra are finally formed. The current synthetic strategy apparently has the potential of synthesizing interesting MOF nanostructures with high index facets besides current well-defined hollow nanocages, which will be further explored for more functions.

The permanent porosity of the as-obtained NPs was confirmed by nitrogen adsorption–desorption isotherms and pore size distribution measurements (Figure S12). As shown in Figure S12a, both Fe^{III}-ICP and Fe^{III}-MOF-5 exhibit a typical type IV sorption isotherm, indicating the mesoporosity of the NPs.[30] In addition, it was observed that nitrogen uptake displays an obvious increase at a low relative pressure ($P/P_0 < 0.01$), suggesting the presence of inherent micropores in these hollow nanocages.[25] The pore size distribution calculated from the BJH method using the desorption branch (Figure S12b) shows that the shells of Fe^{III}-ICP (Fe^{III}-MOF-5) mainly contain mesopores with diameters of approximately 3.8 nm (3.9 nm), which could be further confirmed by their corresponding adsorption branch (Figure S12c,d). Owing to the contribution of mesopores and micropores in the NPs, together with their hollow features, Fe^{III}-ICP (Fe^{III}-MOF-5) shows a large BET surface area of $128\ m^2 g^{-1}$ ($484\ m^2 g^{-1}$) and a Langmuir surface area of $174\ m^2 g^{-1}$ ($661\ m^2 g^{-1}$). The formation of mesopores in the shells of the NPs presumably originate from the voids between coordination polymer aggregates in the shells.[27]

The simple process reported herein can be conveniently used to produce hollow nanostructures not only from pure solid MOF (ICP) but also from various MOF (or ICP)-coated composite NPs with various shapes and sizes. As shown in Figure 4a and Figure S15, the addition of pre-synthesized

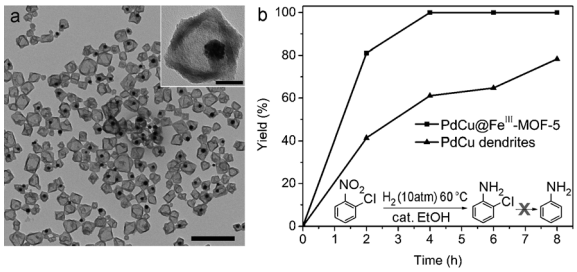

Figure 4. a) TEM image of PdCu@Fe^{III}-MOF-5 yolk–shell structures (scale bar 500 nm; scale bar in the inset 50 nm). b) Yield (%) as a function of time in the selective hydrogenation of 1-chloro-2-nitrobenzene with PdCu dendrites and PdCu@Fe^{III}-MOF-5 yolk-shell structures.

noble-metal NPs (such as Pt, Pd, Au, and PdCu alloys; Figure S14) into the reaction system of Fe^{III}-MOF-5 (or Fe^{III}-ICP) yielded yolk–shell noble-metal@Fe^{III}-MOF-5 (or Fe^{III}-ICP) nanostructures. Shortening the reaction time furnished the formation of core–shell noble-metal@Fe^{III}-MOF-5 nanostructures, which can be firmly confirmed by the case of core–shell PdCu dendrite alloys@Fe^{III}-MOF-5 nanostructures (Figure S16). This further supports our proposed formation mechanism of hollow nanocages. In the reaction solution, PVP not only acts as stabilizer, but also provides the NPs with an enhanced affinity to Fe^{III}-MOF-5 (or Fe^{III}-ICP) through weak coordination interactions between pyrrolidone rings (C=O) and metal ions (Fe^{3+}/Zn^{2+}).[19] Close observation reveals that the encapsulation process has no influence on the structure of the nanocrystals, regardless of the initial sizes and shapes including dendrites, concaves, and round-shaped nanocrystals with sizes ranging from several nanometers to tens of nanometers.

To demonstrate the structural advantage of these yolk–shell composites in catalysis, the selective hydrogenation of 1-chloro-2-nitrobenzene, a challenging reaction and an important industrial process, was chosen as a laboratory test

reaction. Figure 4b shows the kinetic curves for PdCu@Fe^{III}-MOF-5 yolk–shell structures and PdCu dendrites. Noticeably, PdCu@Fe^{III}-MOF-5 yolk–shell structures exhibit much higher activity than PdCu dendrites. The total consumption of 1-chloro-2-nitrobenzene was found within four hours for PdCu@Fe^{III}-MOF-5, in comparison with a maximum conversion of 78% during 8 h over PdCu dendrites. Additionally, it is noted that the selectivity to 2-chloroaniline over PdCu@Fe^{III}-MOF-5 could still retain 100% even after full conversion of 1-chloro-2-nitrobenzene, indicating the complete inhibition of hydro-dechlorination as a side reaction. According to the above results, we suggest that the superior catalytic performance of PdCu@ Fe^{III}-MOF-5 may be ascribed to the construction of a hollow octahedral nanostructure, which can serve as a confined nanoreactor for catalysis, or hydrogen storage in the shells to accelerate the hydrogenation process.[31,32]

In summary, we have successfully prepared a series of well-defined MOF (MOF-5, Fe^{II}-MOF-5, Fe^{III}-MOF-5) and Fe^{III}-ICP hollow nanocages through an one-pot solvothermal approach. Fascinatingly, the addition of pre-synthesized PVP-capped noble-metal nanoparticles into the synthetic solution of MOF (ICP) hollow nanocages yields the yolk–shell noble-metal@MOF (ICP) composite nanostructures. The current research extends the synthetic strategy and methodic versatility for further development of nano-MOFs, especially with hollow and heterometallic structures. Selective hydrogenation tests of 1-chloro-2-nitrobenzene indicate that the design of yolk–shell structures is in favor of achieving excellent catalytic performance as compared to the pure noble-metal nanocrystals. Our results here have demonstrated a great potential in catalyzing organic reactions.

Received: October 2, 2013
Published online: November 28, 2013

Keywords: catalysis · hollow nanostructures · metal–organic frameworks · noble metals · organic–inorganic hybrid composites

[1] H. Li, M. Eddaoudi, M. O'Keeffe, O. M. Yaghi, *Nature* **1999**, *402*, 276 – 279.
[2] S. Kitagawa, R. Kitaura, S. Noro, *Angew. Chem.* **2004**, *116*, 2388 – 2430; *Angew. Chem. Int. Ed.* **2004**, *43*, 2334 – 2375.
[3] G. Férey, *Chem. Soc. Rev.* **2008**, *37*, 191 – 214.
[4] J. P. Zhang, Y. B. Zhang, J. B. Lin, X. M. Chen, *Chem. Rev.* **2012**, *112*, 1001 – 1033.
[5] J. R. Li, J. Sculley, H. C. Zhou, *Chem. Rev.* **2012**, *112*, 869 – 932.
[6] K. Sumida, D. L. Rogow, J. A. Mason, T. M. McDonald, E. D. Bloch, Z. R. Herm, T. H. Bae, J. R. Long, *Chem. Rev.* **2012**, *112*, 724 – 781.
[7] O. K. Farha, A. O. Yazaydin, I. Eryazici, C. D. Malliakas, B. G. Hauser, M. G. Kanatzidis, S. T. Nguyen, R. Q. Snurr, J. T. Hupp, *Nat. Chem.* **2010**, *2*, 944 – 948.
[8] T. H. Bae, J. S. Lee, W. L. Qiu, W. J. Koros, C. W. Jones, S. Nair, *Angew. Chem.* **2010**, *122*, 10059 – 10062; *Angew. Chem. Int. Ed.* **2010**, *49*, 9863 – 9866.
[9] A. Aijaz, A. Karkamkar, Y. J. Choi, N. Tsumori, E. Ronnebro, T. Autrey, H. Shioyama, Q. Xu, *J. Am. Chem. Soc.* **2012**, *134*, 13926 – 13929.
[10] J. S. Seo, D. Whang, H. Lee, S. I. Jun, J. Oh, Y. J. Jeon, K. Kim, *Nature* **2000**, *404*, 982 – 986.
[11] Y. Liu, W. M. Xuan, Y. Cui, *Adv. Mater.* **2010**, *22*, 4112 – 4135.
[12] K. M. L. Taylor-Pashow, J. D. Rocca, Z. G. Xie, S. Tran, W. B. Lin, *J. Am. Chem. Soc.* **2009**, *131*, 14261 – 14263.
[13] P. Horcajada, R. Gref, T. Baati, P. K. Allan, G. Maurin, P. Couveur, G. Ferey, R. E. Morris, C. Serre, *Chem. Rev.* **2012**, *112*, 1232 – 1268.
[14] K. A. White, D. A. Chengelis, K. A. Gogick, J. Stehman, N. L. Rosi, S. Petoud, *J. Am. Chem. Soc.* **2009**, *131*, 18069 – 18071.
[15] S. H. Han, Y. H. Wei, C. Valente, I. Lagzi, J. J. Gassensmith, A. Coskun, J. F. Stoddart, B. A. Grzybowski, *J. Am. Chem. Soc.* **2010**, *132*, 16358 – 16361.
[16] S. L. Qiu, G. S. Zhu, *Coord. Chem. Rev.* **2009**, *253*, 2891 – 2911.
[17] Y. J. Cui, Y. F. Yue, G. D. Qian, B. L. Chen, *Chem. Rev.* **2012**, *112*, 1126 – 1162.
[18] M. Oh, C. A. Mirkin, *Nature* **2005**, *438*, 651 – 654.
[19] G. Lu, S. Z. Li, Z. Guo, O. K. Farha, B. G. Hauser, X. Y. Qi, Y. Wang, X. Wang, S. Y. Han, X. G. Liu, J. S. DuChene, H. Zhang, Q. C. Zhang, X. D. Chen, J. Ma, S. C. J. Loo, W. D. Wei, Y. H. Yang, J. T. Hupp, F. W. Huo, *Nat. Chem.* **2012**, *4*, 310 – 316.
[20] L. C. He, Y. Liu, J. Z. Liu, Y. S. Xiong, J. Z. Zheng, Y. L. Liu, Z. Y. Tang, *Angew. Chem.* **2013**, *125*, 3829 – 3833; *Angew. Chem. Int. Ed.* **2013**, *52*, 3741 – 3745.
[21] a) C. W. Huang, J. C. Jiang, M. Y. Lu, L. Sun, E. I. Meletis, Y. W. Hao, *NanoLett.* **2009**, *9*, 4297 – 4301; b) S. E. Skrabalak, J. Y. Chen, Y. G. Sun, X. M. Lu, L. Au, C. M. Cobley, Y. N. Xia, *Acc. Chem. Res.* **2008**, *41*, 1587 – 1595; c) R. Qiao, X. L. Zhang, R. Qiu, J. C. Kim, Y. S. Kang, *Chem. Mater.* **2007**, *19*, 6485 – 6491; d) K. M. Nam, J. H. Shim, H. Ki, S. I. Choi, G. Lee, J. K. Jang, Y. Jo, M. H. Jung, H. Song, J. T. Park, *Angew. Chem.* **2008**, *120*, 9646 – 9650; *Angew. Chem. Int. Ed.* **2008**, *47*, 9504 – 9508.
[22] a) Z. Y. Wang, D. Y. Luan, F. Y. C. Boey, X. W. Lou, *J. Am. Chem. Soc.* **2011**, *133*, 4738 – 4741; b) L. I. Hung, C. K. Tsung, W. Y. Huang, P. D. Yang, *Adv. Mater.* **2010**, *22*, 1910 – 1914; c) Y. D. Yin, R. M. Rioux, C. K. Erdonmez, S. Hughes, G. A. Somorjai, A. P. Alivisatos, *Science* **2004**, *304*, 711 – 714; d) X. W. Lou, L. A. Archer, Z. C. Yang, *Adv. Mater.* **2008**, *20*, 3987 – 4019; e) L. Zhang, H. B. Wu, S. Madhavi, H. H. Hng, X. W. Lou, *J. Am. Chem. Soc.* **2012**, *134*, 17388 – 17391; f) L. Zhang, H. B. Wu, X. W. Lou, *J. Am. Chem. Soc.* **2013**, *135*, 10664 – 10672.
[23] R. Ameloot, F. Vermoortele, W. Vanhove, M. B. J. Roeffaers, B. F. Sels, D. E. De Vos, *Nat. Chem.* **2011**, *3*, 382 – 387.
[24] J. Huo, L. Wang, E. Irran, H. Yu, J. M. Gao, D. S. Fan, B. Li, J. J. Wang, W. B. Ding, A. M. Amin, C. Li, L. Ma, *Angew. Chem.* **2010**, *122*, 9423 – 9427; *Angew. Chem. Int. Ed.* **2010**, *49*, 9237 – 9241.
[25] Y. Y. Karabach, M. F. C. Guedes da Silva, M. N. Kopylovich, B. Gil-Hernandez, J. Sanchiz, A. M. Kirillov, A. J. L. Pombeiro, *Inorg. Chem.* **2010**, *49*, 11096 – 11105.
[26] W. Cho, H. J. Lee, M. Oh, *J. Am. Chem. Soc.* **2008**, *130*, 16943 – 16946.
[27] S. L. Zhong, R. Xu, L. F. Zhang, W. G. Qu, G. Q. Gao, X. L. Wu, A. W. Xu, *J. Mater. Chem.* **2011**, *21*, 16574 – 16580.
[28] A. M. Spokoyny, D. Kim, A. Sumrein, C. A. Mirkin, *Chem. Soc. Rev.* **2009**, *38*, 1218 – 1227.
[29] H. X. Lin, Z. C. Lei, Z. Y. Jiang, C. P. Hou, D. Y. Liu, M. M. Xu, Z. Q. Tian, Z. X. Xie, *J. Am. Chem. Soc.* **2013**, *135*, 9311 – 9314.
[30] D. P. Serrano, J. Aguado, J. M. Escola, J. M. Podriguez, A. Peral, *Chem. Mater.* **2006**, *18*, 2462 – 2464.
[31] Z. C. Zhang, X. Zhang, Q. Y. Yu, Z. C. Liu, C. M. Xu, J. S. Gao, J. Zhuang, X. Wang, *Chem. Eur. J.* **2012**, *18*, 2639 – 2645.
[32] S. Proch, J. Herrmannsdorfer, R. Kempe, C. Kern, A. Jess, L. Seyfarth, J. Senker, *Chem. Eur. J.* **2008**, *14*, 8204 – 8212.

